JOURNAL OF SPACECRAFT AND ROCKETS
Vol. 52, No. 4, July–August 2015

Plasmonic Force Space Propulsion

Joshua L. Rovey,* Paul D. Friz,† Changyu Hu,‡ Matthew S. Glascock,§ and Xiaodong Yang¶
Missouri University of Science and Technology, Rolla, Missouri 65409

DOI: 10.2514/1.A33155

Plasmonic space propulsion uses solar light focused onto deep-subwavelength nanostructures to excite strong optical forces that accelerate and expel nanoparticle propellant. Simulations predict that light within the solar spectrum can excite asymmetric nanostructures to create plasmonic forces that will accelerate and expel nanoparticles. A peak force of 55 pN/W is predicted for a 50-nm-wide, 400-nm-long nanostructure that resonates at 500 nm. Results for a conceptual design of a plasmonic thruster that has 35 layers, 86 array columns, a multistage length of 5 mm, a 5-cm-diam light focusing lens, and uses 100 nm polystyrene nanoparticles expelled at a rate of 1×10^6 per second would have a thrust of 250 nN, specific impulse of 10 s, and minimum impulse bit of 50 pN · s.

Nomenclature

A	=	area, m^2
B	=	magnetic field, T
E	=	electric field, V/m
F	=	force, N
I	=	intensity, W/m^2
I_{sp}	=	specific impulse, s
L	=	acceleration length, m
N	=	number of array elements
P	=	power, W
T	=	thrust, N
T_{ij}	=	Maxwell stress tensor
f	=	expulsion rate, s^{-1}
g_0	=	gravitational constant, 9.81 m/s^2
m	=	mass, kg
$\dot{m}$	=	mass flow rate, kg/s
v	=	velocity, m/s
δ_{ij}	=	Kronecker delta function
ϵ_o	=	permittivity of free space
μ_0	=	permeability of free space

I. Introduction

INTEREST in small spacecraft continues to increase in government, commercial, and academic sectors. According to a recent SpaceWorks report on the nano/microsatellite market, the number of small satellites being developed and launched will continue to increase over the next 7–10 years from 35 launched in 2012 to an anticipated 188 launched in 2020 [1]. Defense and intelligence interest in nanosatellites is expected to increase from only 8% of launches today to almost 40% by 2015. The recent U.S. Air Force Global Horizons report specifically lists fractionated constellations of small spacecraft as a game-changing technology of focus over the next 15–20 years [2]. NASA continues to develop science and exploration mission scenarios for small spacecraft,** such as asteroid mapping, Earth-observing deployable x-ray telescopes, exoplanet observatories, and constellations of spacecraft for Earth and deep space observations.

In spite of the intense and exploding interest in small spacecraft, their full potential remains untapped because they lack maneuverability. The major challenge remains propulsion. Micci and Ketsdever [3] compiled micropropulsion state of the art in 2000, and many of those micropropulsion systems have been or are being investigated for small spacecraft (e.g., microresistojets, microcavity discharge thrusters, mini-ion/Hall pulsed plasma thrusters, and electrospray). New concepts have also been investigated (e.g., nanoparticle field extraction, laser ablation, and free molecule resistojet). Although significant advances have been made, small spacecraft still lack propulsion for the same reasons outlined by Micci and Ketsdever: mass, power, and volume constraints. The need remains for a propulsion system that can fit on ever-shrinking small nano/pico-spacecraft platforms.

The following sections describe and analyze a new concept for providing maneuverability for small spacecraft. First, the concept of plasmonic force propulsion is described. Then the concept is analyzed by predicting the strength of the plasmonic force field and the propulsion performance of a conceptual thruster design. Finally, conclusions are drawn based on the analysis.

II. Plasmonic Force Propulsion Concept

The plasmonic force propulsion concept is built upon the growing field of plasmonics, which exploits the unique optical properties of metallic nanostructures to route and manipulate light at nanometer length scales. Plasmonic antennas and lenses can focus optical radiation into intense, engineered, localized field distributions or enable coupling to deep-subwavelength guided modes. Enhanced plasmonic forces enable manipulation and acceleration of nanoparticles, in what is commonly referred to as "optical tweezers" [4–6]. The concept is illustrated in Fig. 1. Sunlight is directly focused onto deep-subwavelength metallic nanostructures through a lens. The resonant interaction and coupling of the light with the nanostructure excites surface plasmon polaritons (i.e., plasmons) that generate a strong gradient optical force field. Nanoparticles (e.g., glass beads or metallic particles) are accelerated by the gradient force field and are expelled from the device at high speeds. Because the optical force field is coupled to the nanostructure through the strong light–matter interaction with surface plasmon polaritons, thrust is generated through momentum exchange with the expelled particles.

Careful examination of Fig. 1 reveals a major benefit of the concept: no electric or spacecraft power required. Solar energy is directly converted into propulsive thrust (jet power); additional solar

Presented as Paper 2014-3757 at the 50th Joint Propulsion Conference, Cleveland, OH, 28–30 July 2014; received 12 September 2014; revision received 2 April 2015; accepted for publication 6 April 2015; published online 8 June 2015.

*Associate Professor of Aerospace Engineering, Mechanical and Aerospace Engineering, 292D Toomey Hall, 400 West 13th Street. Associate Fellow AIAA.

†Graduate Research Assistant, Aerospace Plasma Laboratory, Mechanical and Aerospace Engineering, 160 Toomey Hall, 400 West 13th Street. Student Member AIAA.

‡Graduate Research Assistant, NanoOptics Laboratory, Mechanical and Aerospace Engineering, Toomey Hall, 400 West 13th Street.

§Undergraduate Research Assistant, Aerospace Plasma Laboratory, Mechanical and Aerospace Engineering, 160 Toomey Hall, 400 West 13th Street. Student Member AIAA.

¶Assistant Professor of Mechanical Engineering, Mechanical and Aerospace Engineering, Toomey Hall, 400 West 13th Street.

**Data available online at http://www.nasa.gov/news/budget/index.html (retrieved 10 June 2014).

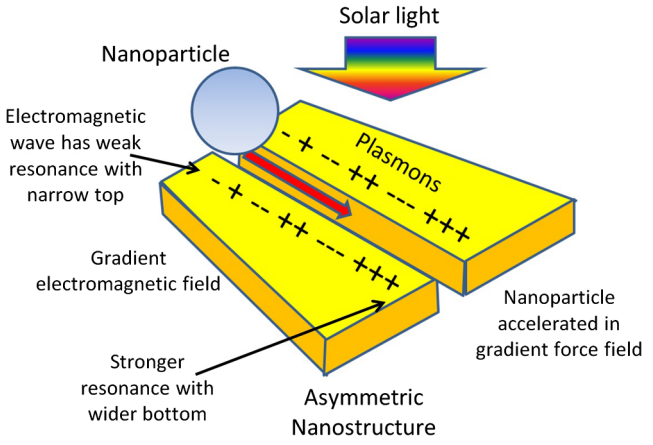

Fig. 1 Schematic of plasmonic force propulsion concept.

cells, batteries, or other energy storage are not required. This has distinct advantages for the mass and power budget of a spacecraft, especially nano- and picosats where mass and power are already severely limited. However, unlike other direct energy conversion propulsion technologies (e.g., solar sails), plasmonic force propulsion is not due to photon pressure, but rather the strong gradient optical force field set up by surface plasmon polaritons excited in the designed metallic nanostructures by the strongly resonant light–matter interaction. This has distinct advantages in terms of the physical size, mass, and performance of the propulsion system. Simulations to predict the strength of the plasmonic force on nanoparticle propellant are described next.

III. Plasmonic Force Predictions

Plasmonic force produced by a three-dimensional nanoscale structure designed to produce a gradient optical force is investigated. A gradient optical force is necessary to expel nanoparticles out of the nanostructure rather than trap them. The numerical model used to predict plasmonic force fields and nanostructure transmission spectra is described. Then simulation results for nanostructures for plasmonic propulsion are presented.

A. Numerical Model

Photon momentum is normally too small to have any significant effect, but in nanoscale structures, the transfer of linear momentum between light and matter can be greatly enhanced. Surface plasmon polaritons (SPPs) confine the electromagnetic waves into a deep-subwavelength scale. Such a strong optical confinement results in significantly enhanced optical field strength and gradient of light field. The strong coupling between the nanostructures SPP mode is supported at the interface of the nanostructures and the nanoparticle. The finite element analysis method (FEM, COMSOL Multiphysics) is used to calculate the optical force of the nanostructure.

The coupling strength determines the optical energy concentration and is related to the gradient optical force generated by the nanostructures. This can be calculated by integrating Maxwell's stress tensor (1) around any arbitrary surface enclosing the nanostructure:

$$T_{ij} \equiv \in_0 \left(E_i E_j - \frac{1}{2}\delta_{ij} E^2 \right) + \frac{1}{\mu_0}\left(B_i B_j - \frac{1}{2}\delta_{ij} B^2 \right) \qquad (1)$$

The indices i and j refer to the coordinates x, y, and z. The stress tensor has a total of nine components (T_{xx}, T_{yy}, T_{xz}, T_{yx}, and so on). The Kronecker delta is represented by δ_{ij}.

Equation (1) is solved using FEM numerical simulation in the COMSOL Multiphysics software. There are several issues related to the numerical simulations of optical forces that must be considered to obtain accurate simulation results. First, the problem of mesh sensitivity has been considered in COMSOL Multiphysics by continuously reducing the grid sizes in the simulation to ensure the achievement of converged optical transmission and force profiles. Second, in the simulation, the sharp corners and edges have been rounded by the COMSOL software during the mesh generation to avoid unrealistic numerical values. Third, optical forces imposed on dielectric nanoparticles due to the plasmonic field of metallic nanostructures are studied. Because the dielectric constant of the nanoparticle will affect the optical resonance of the metallic nanostructure due to the light–matter interaction, the optical response of the whole system, including both the nanoparticle and the metallic nanostructure, must be considered in the numerical simulation to calculate the optical transmission and force. Our simulations include both the nanostructure and the nanoparticle, and results are for the light–matter interaction for the whole system. Fourth, the simulation procedure and results have been verified against experimental data for representative nanostructures. The numerical simulation procedure used in the current paper is the same as was demonstrated in our previous publication [6] with high precision and validity. The FEM numerical simulation of the Maxwell stress tensor has been performed successfully by the authors to study the optical trapping force applied on a single polystyrene nanoparticle of 5 nm diameter [6]. To further validate the current numerical simulation procedure, another recent publication about the optical forces in twisted split ring resonators has been successfully repeated using our simulation [7]. Finally, we have neglected effects such as tribological static charging and photoelectric charging of propellant nanoparticles.

Using the numerical simulation techniques described, Eq. (1) is solved for nanostructure–nanoparticle systems relevant to plasmonic space propulsion. Specifically, optical gradient force is calculated for asymmetric trapezoid nanostructures subjected to light from the solar spectrum from 400 to 1100 nm. This range of the solar spectrum has the highest intensity. Specific nanostructures have been analyzed within the 400–1100 nm range and are described in the following section.

B. Nanostructure Geometry Investigated

Figure 2 shows a two-dimensional (2-D) schematic of the asymmetric trapezoid nanostructures. This asymmetric nanostructure is designed to generate a gradient optical electric field in the presence of light within the 400 – 1100nm band of solar light. Incident light will excite optical resonance of the nanostructure so that gradient optical force will be generated on the nanoparticle (top), and thus the nanoparticle will be accelerated in the negative y direction. The FEM is used to calculate the optical force of the nanostructure on the nanoparticle, using Eq. (1). The nanoparticle is 100 nm and is assumed to be 10 nm above the surface of the nanostructure. The different nanostructures investigated are shown in Fig. 3. All investigated nanostructures are assumed to be gold (Au) nanotrapezoids with a length of 400 nm. Because of the asymmetric structure, the nanoparticle experiences an optical force that is

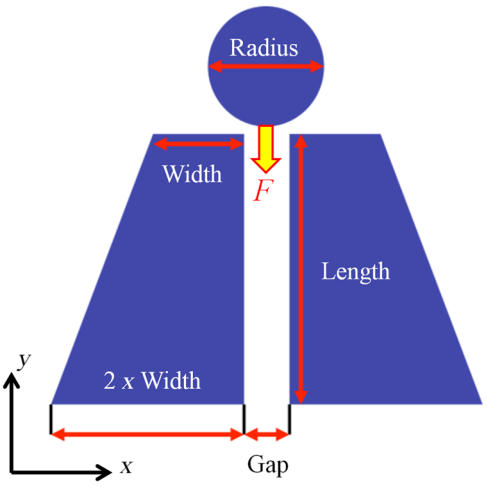

Fig. 2 Schematic of nanoscale asymmetric trapezoid structures.

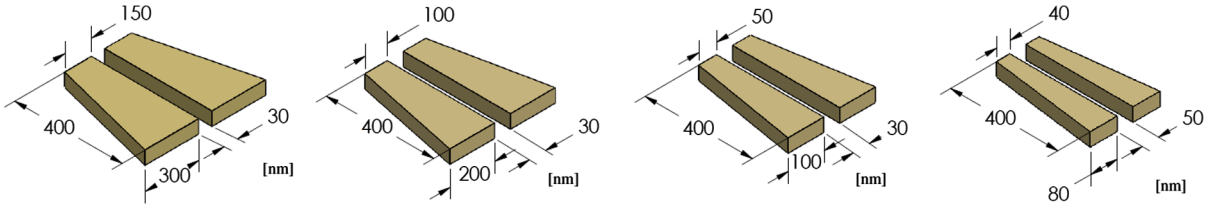

Fig. 3 Schematics of asymmetric metallic nanostructures with different geometry parameters.

dependent on its position along the y axis and moves toward the other side of the nanostructure, in the negative y direction, as shown in Fig. 2. For the desired resonance wavelength, the width of the structures can be tuned so that the strongest optical field concentration inside the metallic structure is achieved. By having nanostructures with different geometry parameters, the most intense region of the solar spectrum (400 – 1100 nm) can be covered.

C. Transmission Spectra and Force Field Results

Transmission spectrums for the investigated nanostructures are shown in Fig. 4. Each nanostructure exhibits a strong resonance within a narrow band (~20 nm) of the solar spectrum. Because of the different dimensions of the nanostructures, each nanostructure resonates at a different wavelength. The four nanostructures investigated have strong resonance at 400, 500, 800, and 1100 nm. The result shows the strong optical resonance from the nanotrapezoid with expected wavelength position. The strong optical resonance in the transmission spectrum indicates the strong light confinement and absorption properties. By using nanostructures with different geometry sizes, broadband solar light from 400 to 1100 nm can be fully used to create strong optical field resonance and therefore gradient optical forces.

Different geometry parameters of trapezoid structures can influence the position of optical resonance wavelength. The width and gap of the nanostructure (as shown in Fig. 2) can be used to tune the optical resonance to different wavelengths within the solar spectrum. The specific dimensions of the investigated nanostructures and their resonant wavelengths are listed in Table 1. Resonant wavelength increases from 400 to 1100 nm as the width of the trapezoid structures increases from 40 to 150 nm, whereas the length is kept constant at 400 nm. The gap size can be tuned from 30 to 50 nm, and it has almost no influence on the resonance wavelength of the nanostructure.

Figure 5 plots the electric field intensity distributions of an asymmetric nanostructure with the width of 100 nm at the resonance wavelengths of 800 nm based on our numerical simulation results. Both the three-dimensional (3-D) and 2-D view are shown in the figure. It is clear that the optical field maximum is located close to the structure end with the large width so that the nanoparticle will be pushed from the end with the small width to the other end with the large width along the y axis. Nanostructures with other geometry parameters supporting different resonance wavelengths have similar optical field distributions.

The optical force on the nanoparticle as a function of its position along the y axis was calculated using Eq. (1) and the results are shown in Fig. 6. The position $y = 0$ nm corresponds to the center of the nanoparticle at the end of the nanostructure with the narrow width. The particle experiences a positive force that increases to a maximum at the other end of the nanostructure (the widest end) and then decreases as the nanoparticle moves away, out of the nanostructure. At the location of approximately 800 nm out from the nanostructure, the nanoparticle starts to experience negative optical force, which means that the nanoparticle will be slightly decelerated, but will still move outward because the net acceleration is positive. Because the net optical force over the entire length (from 0 to 1500 nm) is positive, the nanoparticle will move along one direction and eventually be expelled from the nanostructure.

The force profile $F(y)$ in Fig. 6 for each investigated nanostructure is different because of the different resonant wavelength. The broadband solar spectrum has an irradiance of ~1.85 W/m^2 at

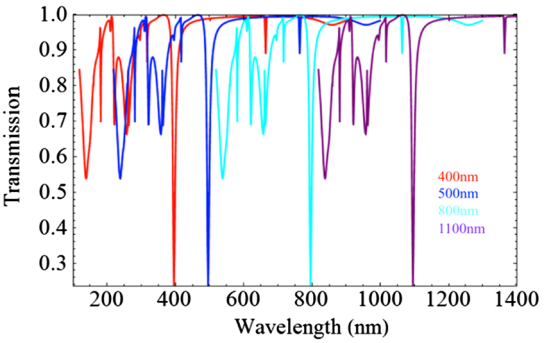

Fig. 4 Transmission spectrums of investigated nanostructures in solar light wavelength range from 400 to 1100 nm.

500 nm and decreases to ~1 W/m^2 at 800 nm. As the incident solar power decreases, the optical force exerted on the nanoparticle also decreases. Each of the nanostructures investigated will receive a different intensity of light based on where its respective resonance wavelength is located within the solar spectrum. The largest optical force, which occurs at the end of the trapezoid structure, increases from 20 to 65 pN/W as the nanostructure resonant wavelength decreases from 1100 to 500 nm, whereas the largest optical force decreases from 65 to 45 pN/W as the resonant wavelength decreases from 500 to 400 nm. Again, these optical force trends are due to the relative optical intensity across the solar spectrum. The result shows that the optical gradient force can accelerate the nanoparticle along y axis in nanotrapezoid structure.

IV. Plasmonic Propulsion Performance Predictions

The preceding nanostructure force profiles were used in an analytical propulsion performance model to predict the thrust and specific impulse of a plasmonic force thruster. Specifically, results were used to develop a conceptual plasmonic force thruster. The impact of important thruster design variables, such as nanoparticle size and mass, nanoparticle exhaust rate, nanostructure array size, and incident power, are presented here.

A. Conceptual Design of a Plasmonic Propulsion Thruster

The general conceptual design of a plasmonic propulsion thruster, based on the knowledge gained from nanostructure simulations, is shown in Fig. 7. It is a layered multistage array of nanostructures. The net force and resulting acceleration of a single nanostructure is very small, only tens of piconewtons per watt (Fig. 5). Multiple nanostructures must be placed end to end (in series, a multistage geometry) to provide an appreciable acceleration of the nanoparticle propellant. This is the multistage length and also the acceleration

Table 1 Different geometry parameters of trapezoid nanostructures for realizing various resonance wavelengths within the solar spectrum from 400 to 1100 nm

Resonance wavelength, nm	Width, nm	Gap, nm	Length, nm
400	40	50	400
500	50	30	400
800	100	30	400
1100	150	30	400

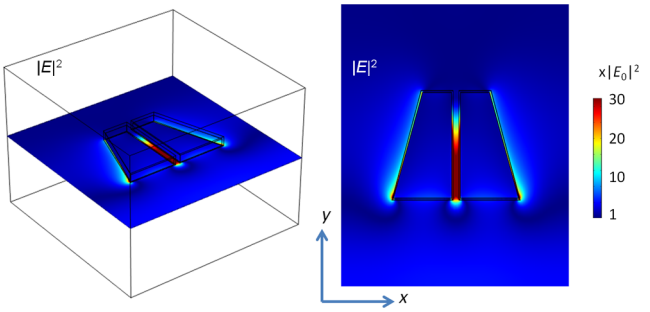

Fig. 5 Electric field intensity distributions of asymmetric nanostructure with width of 100 nm at resonance wavelength of 800 nm. Both 3-D and 2-D views are shown.

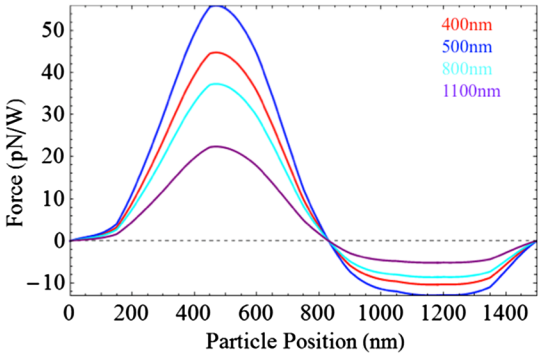

Fig. 6 Calculated optical forces exerted on the nanoparticle by nanostructures designed to resonate at 400, 500, 800, and 1100 nm within the solar spectrum.

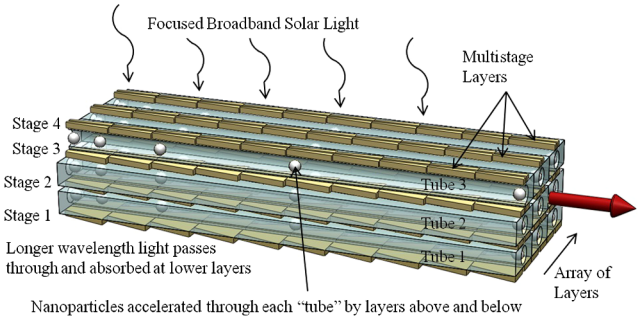

Fig. 7 Conceptual design of a plasmonic force thruster.

length L. A layered structure is beneficial for efficient use of solar light. Nanostructures on top resonate with shorter wavelengths of the solar spectrum, whereas the longer wavelengths pass through to resonate with deeper layers. We assume that the transmission properties of each layer are as given in the preceding numerical simulations (Fig. 4). A structure with four layers is shown in Fig. 7, but transmission spectra results (Fig. 4) show that the absorption/resonant band is very narrow (~20 nm) for a particular nanostructure. This means that many more layers can be used, and the following analysis assumes 36 layers each with a 20 nm resonance band within the 400 – 1100 nm solar broadband. In between each layer is a nanoparticle guide tube. Nanoparticle propellant is accelerated and expelled from the guide tube by plasmonic forces applied by the nanostructure layers directly above and below it. The following analysis assumes there are 36 layers of nanostructures with 35 guide tubes in between. This layered multistage structure is repeated (columns) to form a large array of N elements, where $N =$ layers (rows) x columns. The area solar light is incident upon is the thruster area A_{thruster} and is the acceleration length L times the number of columns in the array. Not shown in Fig. 7 is the solar light focusing lens.

B. Analytical Propulsion Performance Model

The performance of a plasmonic thruster was analytically modeled based on the design parameters of the conceptual model shown in Fig. 7. Specifically, both thrust and specific impulse are predicted using fundamental physics models. Solar light power incident on the thruster is dependent on the focusing lens diameter (area A_{lens}) as shown in Eq. (2), where I is solar intensity in low Earth orbit (1.4 kW/m^2). The solar light power incident on a single nanostructure that makes up the thruster array is given by Eq. (3). It is clear from this relationship that maximizing the collection lens size and minimizing the thruster area increases the power incident on each individual nanostructure, which increases the accelerating plasmonic force on the nanoparticle propellant (Fig. 5):

$$P_{\text{thruster}} = IA_{\text{lens}} \tag{2}$$

$$P_{\text{nanostructure}} = P_{\text{thruster}} \frac{A_{\text{nanostructure}}}{A_{\text{thruster}}} = I \frac{A_{\text{lens}} A_{\text{nanostructure}}}{A_{\text{thruster}}} \tag{3}$$

Incident solar light excites SPPs in each nanostructure of the thruster array, resulting in an optical force on the nanoparticle propellant as given by Fig. 6. The force is a function of position within each individual nanostructure and is therefore a function of position along the entire multistage series of nanostructures $F(y)$. The force profile for an individual nanostructure is given by the results of the simulations shown in Fig. 6. This single nanostructure force profile is assumed to be the same for each nanostructure constituting the entire multistage assembly of nanostructures. Additionally, the force profile is different for each layer of the multistage geometry. That is, each layer has a nanostructure with different dimensions to resonate with a different desired bandwidth of the solar spectrum, and, as a result of the relative intensity across the solar spectrum and the efficiency of different nanostructure geometry, the force profile is different for each layer, as shown in Fig. 6. We extrapolate the results to all 36 layers, scaling the force profile of each layer based on its wavelength of resonance.

The final velocity of the nanoparticle propellant is calculated using Eq. (4), where v_i is the final velocity (assuming zero initial velocity) of the nanoparticle out of tube i, $F_{\text{above,below}}(y)$ is the force profile associated with the multistage nanostructure layer above or below the nanoparticle guide tube, L is the length of the multistage nanostructure, and m is the mass of the nanoparticle. Each layer of the thruster is expelling nanoparticles at a different velocity because the plasmonic force on the nanoparticle is different for each nanostructure geometry:

$$\frac{v_i^2}{2} = \int_0^L \frac{F_{\text{above}}(y) + F_{\text{below}}(y)}{m}\,\mathrm{d}y \tag{4}$$

The total thrust force T of the thruster array is the sum of the thrust produced by each individual tube expelling nanoparticles. Each layer is expelling nanoparticles at a different velocity, but the model assumes each tube is expelling nanoparticles with the same mass m and at the same rate f. The thrust can be calculated using Eq. (5), where N is the number of guide tubes in the array (the size of the array) and f is the rate at which the nanoparticles are being expelled from each tube (per second). Specific impulse I_{sp} is calculated using Eq. (6), where $g_0 = 9.81$ m/s^2:

$$T = \sum_i^N \dot{m}\, v_i = \sum_i^N mf v_i \tag{5}$$

$$I_{\text{sp}} = \frac{T}{\dot{m} g_0} = \frac{T}{Nmf g_0} \tag{6}$$

C. Propulsion Performance Results

The following sections describe results from the propulsion performance model. Specifically, the effects of particle mass (size and density, $m = \rho V$), acceleration length L, expulsion rate f, array size N, and collection lens size A_{lens} on propulsion performance (T, I_{sp}) are investigated.

Preliminary analysis using representative force profile data offers a good basis to determine how the key performance characteristics will depend on the constraints of the plasmonic simulations, as well as characteristics of the nanoparticle. Thrust force and specific impulse directly depend on the mass, and thus implicitly the density and size of the nanoparticle being expelled. Gold, glass, and polystyrene nanoparticles are investigated because these are commonly used in nanooptics and plasmonic experiments. Figure 8 shows a comparison of nanoparticle mass relative to size (diameter) of the particles.

The effect of nanoparticle type and size on propulsion performance is shown in Fig. 9. The analysis assumes a 5 mm acceleration length L, particle expulsion rate f of 1×10^6 per second, array size N of $\sim 3000(35 \times 86)$, and a 5-cm-diam focusing lens A_{lens}. The feasibility of these parameters is discussed in a following section. Results show that thrust increases while specific impulse decreases as the nanoparticle diameter increases. The lighter polystyrene nanoparticles have higher specific impulse but correspondingly lower thrust.

Increasing the acceleration length L does not alter the thrust or specific impulse. A longer acceleration length does increase the thrust and the specific impulse for a constant incident light power, as shown in Eq. (4). However, as acceleration length increases, the total area of the nanostructure array (i.e., A_{thruster}) also increases. As Eq. (3) shows, this will reduce the power incident on the thruster, resulting in decreased plasmonic force. The increase provided by longer acceleration length is canceled by the decrease in light power incident on the thruster.

An identical trend is found for the array size N. Increasing the array size N does not alter the thrust or specific impulse. A larger array size would increase thrust for a constant incident light power, as shown in Eq. (5), but as array size increases, the total area of the nanostructure array (i.e., A_{thruster}) also increases. As Eq. (3) shows, this reduces the power incident on the thruster, resulting in decreased plasmonic force. The increase provided by a larger array is canceled by the decrease in light power incident on the thruster.

Expulsion rate f does directly impact the thrust, but has no impact on specific impulse, as shown in Eqs. (5) and (6). Thrust increases linearly with expulsion rate. Specific impulse is a measure of the exit velocity, and the rate at which particles are being expelled does not affect their final velocity. Expulsion rate is estimated to be 1×10^6 per second for the analysis here, based on previous studies of nanoparticle extraction using gas jets [8].

Thrust and specific impulse are greatly affected by the light power incident on the nanostructures. That is, by the size of the collection lens used to focus solar light onto the thruster A_{lens}. There is a linear relationship between lens diameter and thrust and specific impulse, as shown in Fig. 10. This is a direct result of Eq. (3), where the lens area directly increases the incident power on the thruster, which increases the plasmonic force, total nanoparticle acceleration, exit velocity, specific impulse, and thrust. The relationship is linear because of the proportionalities in the preceding equations, which is summarized here. The solar power incident on the thruster is proportional to the lens area, which is proportional to the square of the lens diameter Eq. (3). The power incident on the thruster is also proportional to the plasmonic force generated by the nanostructures, which is proportional to the square of the exit velocity [Eq. (4)] and square of the specific impulse and thrust [Eqs. (5) and (6)]. Therefore, lens diameter should be linearly related to the thrust and specific impulse, which is what the model results show (Fig. 10).

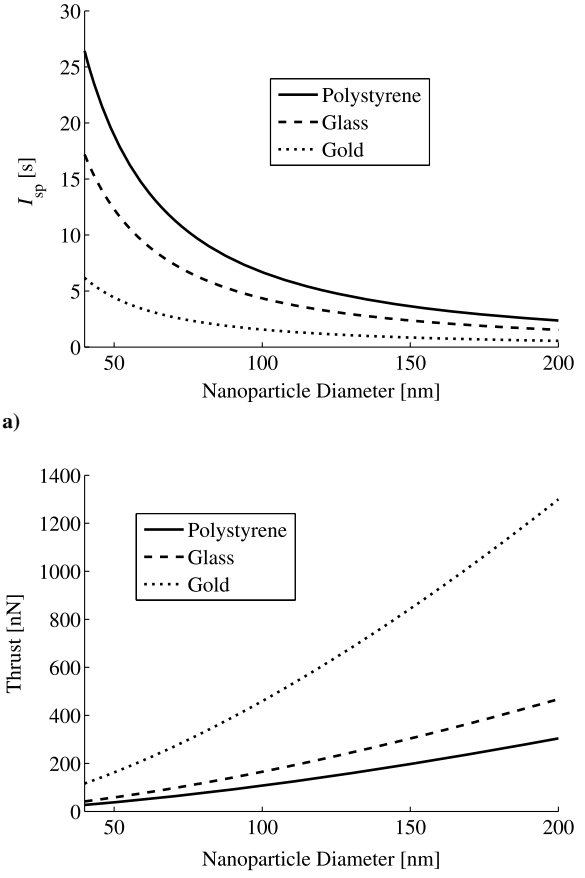

Fig. 9 Performance analysis of conceptual plasmonic thruster.

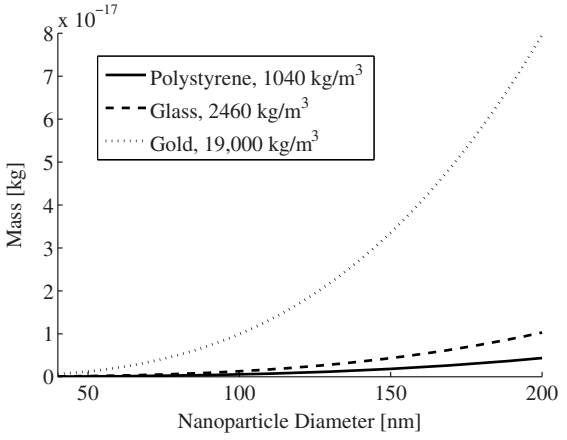

Fig. 8 Comparison of mass of possible nanoparticle propellants with variation in particle diameter.

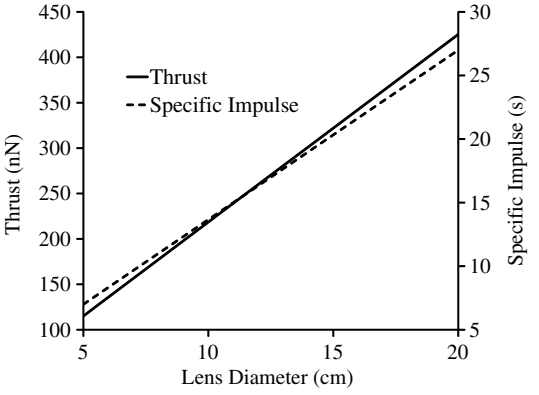

Fig. 10 Specific impulse and thrust vs lens diameter for 100 nm polystyrene nanoparticles.

V. Conclusions

Results from numerical simulations support the fundamental principle of the plasmonic force space propulsion concept. Simulations predict that light within the solar spectrum can excite asymmetric nanostructures to create plasmonic forces that will accelerate and expel nanoparticles (Fig. 6), generating a thrust force. Simulation results of the light–matter interaction show that the resonance bounds for a single nanostructure can be tuned by changing the nanostructure geometry. For instance, a 40-nm-wide, 400-nm-long nanostructure will resonate at 400 nm, whereas a 150-nm-wide, 400-nm long nanostructure will resonate at 1100 nm (Table 1). Further, the resonance bandwidth for a single nanostructure is only about 3% (∼20 nm) of the strongest band of the solar spectrum (400–1100 nm) (Fig. 4). The force profile of a single nanostructure is similar for the different geometry investigated, but the magnitude changes. For instance, a 40-nm-wide, 400-nm-long nanostructure has a peak force of 44 pN/W, whereas a 150-nm-wide, 400-nm long nanostructure has a peak force of 22 pN/W (Fig. 6). This effect is due to the variation in intensity of the solar spectrum at the resonance wavelength for the different geometry.

Results have elucidated the design geometry and configuration for a plasmonic force propulsion thruster and have led to a conceptual design. A single plasmonic force propulsion thruster should consist of many individual asymmetric nanostructures arranged in a multistage, layered array. Nanostructures should be arranged end to end in series to form a multistage because a single nanostructure produces very small force (∼10 pN/W, Fig. 6) and multiple stages are necessary to achieve useable thrust and exit velocity. Multistage nanostructures should be layered (i.e., stacked) on top of each other. Each layer should be designed to resonate at a different wavelength within the broadband solar spectrum. This will maximize use of the broadband solar spectrum because shorter wavelength light is absorbed/resonates with top layers, whereas longer wavelength light passes through to resonate with lower layers. Finally, the multistage layers of nanostructures should be repeated in an array to provide increased thrust.

Results for a conceptual design of a plasmonic thruster that has 35 layers, 86 array columns, a multistage length of 5 mm, a 5-cm-diam light focusing lens, and uses 100 nm polystyrene nanoparticles expelled at a rate of 1×10^6 per second would have a thrust of 250 nN, specific impulse of 10 s, and minimum impulse bit of 50 pN · s.

Acknowledgments

The authors would like to thank the NASA Innovative Advanced Concepts program for partially supporting this work through grant NNX13AP78G. This work was also partially supported through U.S. Air Force Office of Scientific Research grant FA9550-14-1-0230, Mitat Birkan program monitor. Additionally, P. D. Friz would like to thank the Missouri Space Grant Consortium for sponsoring his graduate program, and M. S. Glascock would like to thank the Missouri University of Science and Technology Opportunities for Undergraduate Research Experiences program for sponsoring his undergraduate project.

References

[1] DePasquale, D., and Bradford, J., *Nano/Microsatellite Market Assessment*, SpaceWorks, Atlanta, Feb. 2013, pp. 6–9.

[2] Maybury, M. T., "Global Horizons: United States Air Force Global Science and Technology Vision," U.S. Air Force, AF/ST TR-13-01, United States Air Force Chief Scientist, Washington, D.C., June 2013, pp. 11–14.

[3] Micci, M. M., and Ketsdever, A. D., *Micropropulsion for Small Spacecraft*, edited by Zarchan, P., Vol. 187, Progress in Aeronautics and Astronautics, AIAA, Reston, VA, 2000, pp. 45–126.

[4] Juan, M. L., Righini, M., and Quidant, R., "Plasmon Nano-Optical Tweezers," *Nature Photonics*, Vol. 5, No. 6, 2011, pp. 349–356. doi:10.1038/nphoton.2011.56

[5] Schuller, J. A., Barnard, E. S., Cai, W., Jun, Y. C., White, J. S., and Brongersma, M. L., "Plasmonics for Extreme Light Concentration and Manipulation," *Nature Materials*, Vol. 9, No. 3, 2010, pp. 193–204. doi:10.1038/nmat2630

[6] Yang, X., Liu, Y., Oulton, R. F., Yin, X., and Zhang, X., "Optical Forces in Hybrid Plasmonic Waveguides," *Nano Letters*, Vol. 11, No. 2, Feb. 2011, pp. 321–328. doi:10.1021/nl103070n

[7] Tang, C., Wang, Q., Liu, F., Chen, Z., and Wang, Z., "Optical Forces in Twisted Split-Ring-Resonator Dimer Stereometamaterials," *Optics Express*, Vol. 21, No. 10, 2013, pp. 11,783–11,792. doi:10.1364/OE.21.011783

[8] Pyatenko, A., Takeuchi, H., Chiba, S., and Ohyama, Y., "Dispersion of Fine Powder Agglomerates Under Microgravity," *AIChE Journal*, Vol. 47, No. 12, Dec. 2001, pp. 2696–2704. doi:10.1002/(ISSN)1547-5905

M. Choudhari
Associate Editor